IEEE Access
Multidisciplinary ⋮ Rapid Review ⋮ Open Access Journal

Received May 5, 2020, accepted May 11, 2020, date of publication May 18, 2020, date of current version June 4, 2020.

Digital Object Identifier 10.1109/ACCESS.2020.2995405

Dual-Band Compact Wilkinson Power Divider Using Common Inductor and Complex Load

CHATRPOL PAKASIRI[1] AND SEN WANG[2], (Member, IEEE)
[1]College of Advanced Manufacturing Innovation, King Mongkut's Institute of Technology Ladkrabang, Bangkok 10520, Thailand
[2]Department of Electronic Engineering, National Taipei University of Technology, Taipei 10608, Taiwan

Corresponding authors: Chatrpol Pakasiri (chatrpol.pa@kmitl.ac.th) and Sen Wang (wangsen@ntut.edu.tw)

This work was supported in part by the Research Funding under the Memorandum of Understanding of King Mongkut's Institute of Technology Ladkrabang under Grant KREF156301, in part by the National Taipei University of Technology-King Mongkut's Institute of Technology Ladkrabang Joint Research Program (NTUT-KMITL) under Grant NTUT-KMITL-107-01, and in part by the Research and Development Center for Smart Textile Technology of NTUT.

ABSTRACT A 1.8/2.4-GHz dual-band compact Wilkinson power divider was designed and implemented using an integrated passive device process. The design used a common inductor to match impedance in the even mode. The common inductor replaced two shunt inductors in the circuit so the circuit size was reduced. An additional complex load was then used for matching impedance in the odd mode. The circuit measurements showed reflection at all ports better than –11.9 dB, isolation at the output ports better than –14 dB and transmission coefficient better than –4.3 dB, at both operating frequencies. The circuit occupied only $0.036\lambda_o \times 0.018\lambda_o$ at the higher operating frequency.

INDEX TERMS Common inductor, dual band, integrated passive device, lumped transmission line, Wilkinson power divider.

I. INTRODUCTION

Power dividers were used in many circuit blocks such as low noise amplifiers, power splitters, array antennas, etc. Dual-band and Multi-band operations are also of great benefits in various applications. Among power dividers, Wilkinson power dividers (WPD) have been studied extensively in both single and dual-band operations. They were implemented in many forms such as printed-circuit board (PCB), CMOS or in an Integrated Passive Device (IPD). On PCB, microstrip transmission lines were normally used in WPD circuits. With larger transmission line traces, this type of WPD can handle the largest power of the three forms mentioned. There are several techniques to design a dual-band Wilkinson power divider (WPD). Distributed transmission lines with periodically loaded slow wave structure were used by Rawat and Ghannouchi to make dual-band WPD [1]. Multi-section transmission lines were also used in some works. Additional lumped components connected in the shunt path were used to make dual-band WPDs [2]–[4]. Stubs instead of lumped components have been used [5]–[8]. Cascaded multi-section transmission lines without shunt components were also implemented [9]–[12]. Composite right-/left-handed transmission lines were also used in dual-band WPDs [13], [14]. All these PCB designs had similar performance with some size differences, which were usually greater than $0.1\lambda_o \times 0.1\lambda_o$.

Beside WPD on PCB forms, some works were also implemented in CMOS process. Chiang, *et al.* used complementary-conducting-strip transmission lines in designing a WPD for Ka-band application [15]. A π-network [16] and T-network [22] lumped circuits were used to replace distributed transmission lines to reduce the circuit sizes in single-band designs but the insertion losses in both designs were relatively high due to low Q inductors. Active inductors were also used in CMOS to reduce the circuit sizes [17], [18]. Since the CMOS substrate was quite lossy, lower performances was expected in passive WPDs. The active ones also suffered from power consumption, noise and nonlinearity issues. Nevertheless, the circuit sizes were much smaller than those of PCB implementations.

WPDs implemented in an IPD process were as small as those of CMOS but had better performance since the inductors implemented had better quality factors. Normally, π-network right-handed transmission lines were common in implementing transmission lines in an IPD. The 900-MHz and 2.4-GHz Wilkinson power dividers based on π-network right-handed transmission lines implemented on

The associate editor coordinating the review of this manuscript and approving it for publication was Yong Chen.

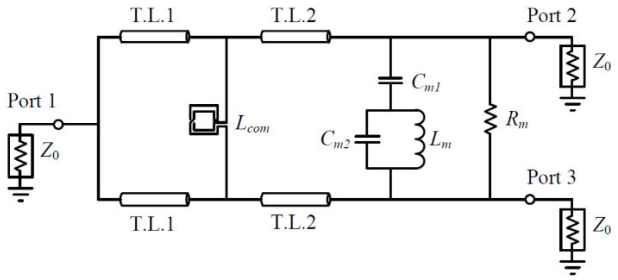

FIGURE 1. Dual-band Wilkinson power divider in distributed form.

GaAs-IPD technology have been shown [19], [20]. In this paper, a dual-band WPD was designed and implemented on IPD process to operate at 1.8 and 2.4 GHz. In addition to π-network right-handed transmission lines, the design included a common inductor and a complex load connecting the output ports. The design used even and odd mode analysis. Combining a common inductor, complex load and two section transmission lines, a compact dual-band WPD was implemented. Note that since there is a trade-off between insertion loss and isolation in practice, design optimization had low insertion loss as the first priority. The detailed analysis and design are discussed in the following sections.

II. COMPACT POWER DIVIDER WITH COMMON INDUCTOR AND COMPLEX LOAD

Conventional power dividers, are usually implemented in distributed transmission lines. For a compact form in integrated circuits, LC-based lumped circuits were used. For a single operating frequency circuit, the transmission lines used can be either λ/4 [17] or 3λ/4 [19]. For a λ/4 line, a π-network lumped transmission line circuit was normally usedwhile a T-network was used for 3λ/4 line. In both cases, the circuits had at least one inductor. Since the size of the inductor greatly impacts the size of the overall circuit, a minimal number of inductors were used, or smaller size inductor were all preferred.

To make the circuit operate at dual-frequency bands, shorter transmission lines with a common inductor and complex load were used. Figure 1 shows the circuit topology. The transmission lines were divided into two sections, T.L.1 and T.L.2. T.L.1 was next to Port 1, while the common inductor was placed in the middle between T.L.1 and T.L.2. The complex load was placed between T.L.2 and Port 2 and Port 3. The circuit was analyzed using the even and odd mode technique. The even and odd mode equivalent circuits are shown in Fig. 2.

The benefits of the common inductor are even mode matching and size reduction. In the even mode, a shunt element along the transmission lines must connect to ground and therefore two elements are needed for the shunt branch between T.L.1 and T.L.2. A smaller common inductor replaced two shunt inductors, since it represented a larger equivalent shunt inductor in the even mode due to the mutual inductance. Therefore, both even matching and circuit size reduction can be achieved. The complex load was designed

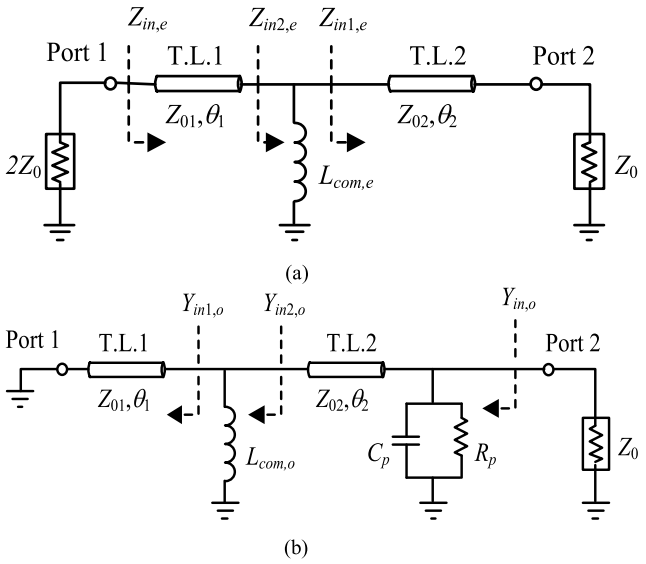

FIGURE 2. Equivalent circuit of Wilkinson power divider in (a) even mode and (b) odd mode.

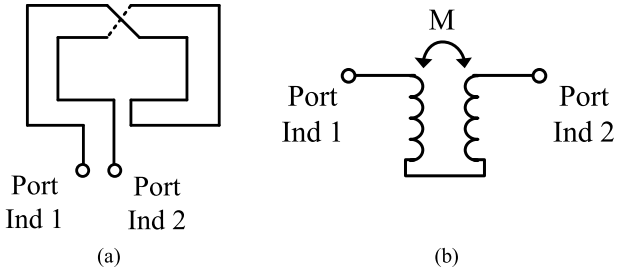

FIGURE 3. Common inductor with (a) layout model and (b) circuit symbol.

to match the impedance in the odd mode at both operating frequencies. The S-parameter requirements of the circuit are

$$S_{11,e} = S_{22,e} = S_{33,e} = 0 \tag{1a}$$
$$S_{11,o} = S_{22,o} = S_{33,o} = 0 \tag{1b}$$
$$|S_{12,e}| = |S_{21,e}| = |S_{13,e}| = |S_{31,e}| = 1 \tag{1c}$$
$$|S_{12,o}| = |S_{13,o}| = 0 \tag{1d}$$
$$S_{23} = S_{32} = 0 \tag{1e}$$

In Fig. 2, the common inductor L_{com} was considered as $L_{com,e}$ and $L_{com,o}$ for the equivalent even- and odd-mode circuit. The $L_{com,e}$ value has been increased in the even mode due to the mutual inductance of the common inductor. The detailed analysis of the common inductor, even and odd modes are considered next.

A. COMMON INDUCTOR

The common inductor can be represented by two-port Z-parameters as shown in Fig. 3. The input signals of both input ports rotate in the same direction and meet each other at the middle of the structure. Physically they can be represented by two inductors with a mutual coupling factor.

As a two-port structure, its Z-parameters at desired frequencies can be extracted by electromagnetic simulation.

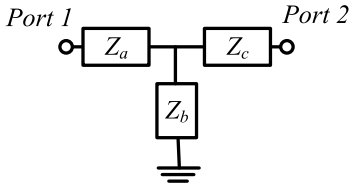

FIGURE 4. An equivalent T-network representing a common inductor.

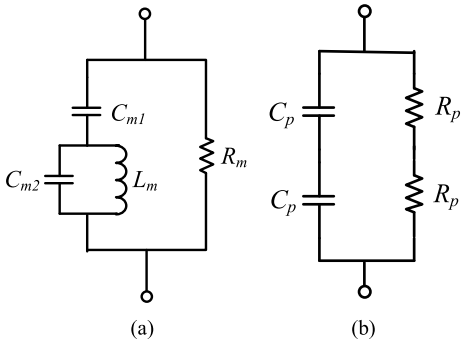

FIGURE 5. Complex load connecting output ports. (a) Complex load network and (b) an equivalent parallel R_P-C_P circuit.

To be used in even- and odd- mode analysis, an equivalent T-network shown in Fig. 4 was used to represent the network. Its components are

$$Z_{a,ind} = Z_{11,ind} - Z_{12,ind} \tag{2a}$$
$$Z_{b,ind} = Z_{12,ind} \tag{2b}$$
$$Z_{c,ind} = Z_{22,ind} - Z_{21,ind} \tag{2c}$$

where the Z-parameters of the inductor is

$$[Z]_{ind} = \begin{bmatrix} Z_{11,ind} & Z_{12,ind} \\ Z_{21,ind} & Z_{22,ind} \end{bmatrix} \tag{2d}$$

B. COMPLEX LOAD

The complex load consists of two capacitors, one inductor and one resistor. Its equivalent circuits of R_p-C_p parallel network were used in the odd mode analysis. Figure 5 shows the complex load and its equivalent circuit for the odd mode analysis. The component values can be found as

$$R_p = R_m/2 \tag{3a}$$
$$C_p = \frac{2\omega C_{m1}\left(1-\omega^2 C_{m2}L_m\right)}{1-\omega^2 L_m\left(C_{m2}-C_{m3}\right)} \tag{3b}$$

The half circuit of Fig. 5(b) was then used in the analysis of the odd mode.

C. EVEN MODE ANALYSIS

In the even mode analysis, port impedance at port 1 becomes twice the normal value. The components included in the even mode are T.L.1, T.L.2 and the common inductor. The complex load has been omitted since there is no current flowing into this branch. Proper values of the remaining components must be chosen so that the input impedances at Port 1 and Port 2 are matched at the dual-band frequencies. In terms of input impedance at Port 1, its value can be found by (4a)-(5b), as shown at the bottom of this page, where Z_{01}, Z_{02}, θ_1, and θ_2 are the characteristic impedances and electrical lengths of T.L.1 and T.L.2 respectively. The matching conditions in the even mode analysis at both frequencies are

$$Z_{in,e,re} = 2Z_0 \tag{6a}$$
$$Z_{in,e,im} = 0 \tag{6b}$$

D. ODD MODE ANALYSIS

In the odd mode analysis, port 1 impedance is replaced with short circuit. The components in the equivalent circuit are T.L.1, T.L.2, common inductor and complex loadas shown in Fig. 2(b). The input impedance at Port 2 is

$$Y_{in,o} = Y_{in,o,re} + jY_{in,o,im} \tag{7a}$$

where, (7b)-(7c) as shown at the bottom of the next page. The matching conditions in the odd mode analysis at both frequencies are

$$Y_{in,o,re} = \frac{1}{Z_0} \tag{8a}$$
$$Y_{in,o,im} = 0 \tag{8b}$$

$$Z_{in,e,re} = \frac{Z_{01}^2 Z_{in2,e,re}\sec^2(\theta_1)}{\left(Z_{01} - Z_{in2,e,im}\tan(\theta_1)\right)^2 + \left(Z_{in2,e,re}\tan(\theta_1)\right)^2} \tag{4a}$$
$$Z_{in,e,im} = \frac{Z_{01}\left[\left(Z_{in2,e,im} + Z_{01}\tan(\theta_1)\right)\left(Z_{01} - Z_{in2,e,im}\tan(\theta_1)\right) - Z_{in2,e,re}^2\tan(\theta_1)\right]}{\left(Z_{01} - Z_{in2,e,im}\tan(\theta_1)\right)^2 + \left(Z_{in2,e,re}\tan(\theta_1)\right)^2} \tag{4b}$$

$$Z_{in2,e,re} = \frac{\omega^2 L_{com,e}^2 Z_0 Z_{02}^2 \sec^2(\theta_2)\left(Z_{02}^2 + Z_0^2\tan^2(\theta_2)\right)}{\left(Z_0 Z_{02}^2\sec^2(\theta_2)\right)^2 + \left(Z_{02}\left(Z_{02}^2 - Z_0^2\right)\tan(\theta_2) + \omega L_{com,e}\left(Z_{02}^2 + Z_0^2\tan^2(\theta_2)\right)\right)^2} \tag{5a}$$
$$Z_{in2,e,im} = \frac{\omega L_{com,e} Z_0^2 Z_{02}^4 \sec^4(\theta_2) + \omega L_{com,e} Z_{02}\tan(\theta_2)\left(Z_{02}^2 - Z_0^2\right)\left[Z_{02}\left(Z_{02}^2 - Z_0^2\right)\tan(\theta_2) + \omega L_{com,e}\left(Z_{02}^2 + Z_0^2\tan^2(\theta_2)\right)\right]}{\left(Z_0 Z_{02}^2\sec^2(\theta_2)\right)^2 + \left(Z_{02}\left(Z_{02}^2 - Z_0^2\right)\tan(\theta_2) + \omega L_{com,e}\left(Z_{02}^2 + Z_0^2\tan^2(\theta_2)\right)\right)^2} \tag{5b}$$

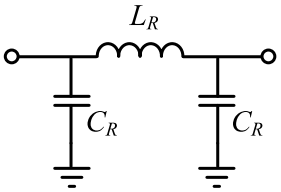

FIGURE 6. A π-network right-handed transmission line.

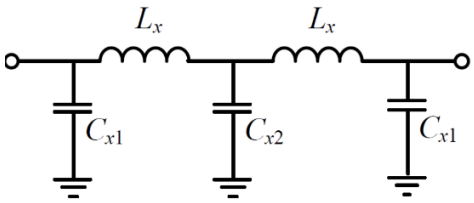

FIGURE 7. Modified lumped transmission line circuit.

With the conditions in (6) and (8), the required specification in (1) can be achieved.

III. TRANSMISSION LINE CIRCUIT WITH LUMPED COMPONENTS

The circuit was implemented in an IPD process with size limitation. Therefore, the conventional distributed transmission lines were replaced by lumped transmission line circuits. A simple lumped transmission line circuit is a π-network right-handed transmission line shown in Fig. 6. The circuit consists of one inductor and two capacitors. At a given electrical length, its characteristic impedance is proportional to the inductor and inversely proportional to the capacitor. Proper values of these components must be considered, since an inductor occupies a large area. This structure has a limitation since its transmission line behavior degrades with its electrical length [21]. In addition, lower Q components contribute to higher insertion loss on the overall circuit. Transmission lines 1 and 2 are considered next.

A. TRANSMISSION LINE 2

Transmission line 2 was chosen to have smaller characteristic impedance than that of the ports. Its electrical length was set to be relatively small so that a simple π-network right-handed transmission line can be used. The components and transmission line properties are related by

$$\theta_2 = \cos^{-1}(1 - \omega^2 L_R C_R) \tag{9a}$$

$$Z_{02} = \frac{\omega L_R}{\sin\left[\cos^{-1}\left(1 - \omega^2 L_R C_R\right)\right]} \tag{9b}$$

If its electrical length at 2.4 GHz is limited at θ_{2x}, then the inductor-capacitor multiplication factor is

$$L_R C_R < \frac{1 - \cos(\theta_{2x})}{\omega_2^2} \tag{10}$$

where ω_2 is the angular frequency at 2.4 GHz. Pakasiri, *et al.* showed that with a low quality factor for the inductor on a lossy substrate, the electrical length of a π-network right-handed transmission line should be less than 60° [21]. Here, transmission line 2 was limited to 50° at the upper frequency band. Since the T.L.2 implementation was a single-section lumped transmission line, its transmission line performance degradation made the overall circuit bandwidth narrower. Wider bandwidth could be achieved with a multi-section T.L.2 [21], but the circuit size would be larger.

B. TRANSMISSION LINE 1

The electrical length of this line was quite long compared to the second line. The modified circuit, shown in Fig. 7, was used so that it acted as a transmission line at both operating frequencies. The electrical length and characteristic impedance of the line are

$$\theta_1 = \cos^{-1}\left[1 - \omega^2\left(C_{x2}L_x + 2C_{x1}L_x\right) + \omega^4 C_{x1}C_{x2}L_x^2\right] \tag{11a}$$

$$Z_{01} = \frac{\omega L_x\left(2 - \omega^2 C_{x2}L_x\right)}{\sin\left[\cos^{-1}\left(1 - \omega^2\left(C_{x2}L_x + 2C_{x1}L_x\right) + \omega^4 C_{x1}C_{x2}L_x^2\right)\right]} \tag{11b}$$

To set a limitation on the electrical length θ_{1x}, a transcendental equation below was applied for determining the capacitors and inductors.

$$\cos^{-1}\left[1 - \omega^2\left(C_{x2}L_x + 2C_{x1}L_x\right) + \omega^4 C_{x1}C_{x2}L_x^2\right] < \theta_{1x} \tag{12}$$

In this work, θ_{1x} was set at 90° at the upper frequency band.

IV. IMPLEMENTATION AND MEASUREMENTS

The circuit was implemented in an IPD. There were three metal layers on a silicon substrate as illustrated in Fig. 8. Dielectrics 1 and 2 had dielectric constant values of 6.7 and 2.65. The metal layers and vias were copper. In the layout, all components, especially inductors, possessed resistance, which effected the transmission line behaviors.

The capacitor layouts were parallel plates using the M1 and M2 layers. The inductors were rectangular spirals. The resistor was in meander trace form. A chip image is in Fig. 9. The layout area was 4.5mm×2.2mm or $0.036\lambda_o \times 0.018\lambda_o$ where λ_o is the wavelength of free space at 2.4 GHz.

$$Y_{in,o,re} = \frac{1}{R_p} \tag{7b}$$

$$Y_{in,o,im}P = j\left[\omega C_p - \frac{Z_{02}\left(\omega L_{com,o} + Z_{01}\tan(\theta_1)\right) - \omega L_{com,o}Z_{01}\tan(\theta_1)\tan(\theta_2)}{Z_{02}\left(\omega L_{com,o}Z_{01}\tan(\theta_1) + \omega L_{com,o}Z_{02}\tan(\theta_2) + Z_{01}Z_{02}\tan(\theta_1)\tan(\theta_2)\right)}\right] \tag{7c}$$

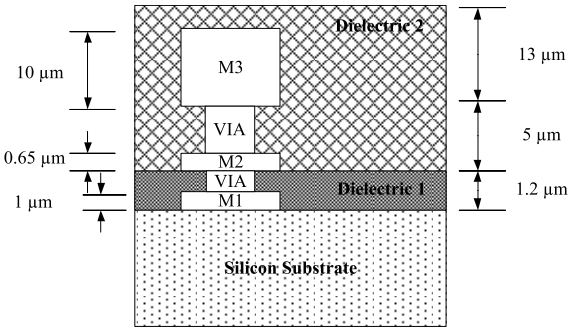

FIGURE 8. Cross section of the IPD process.

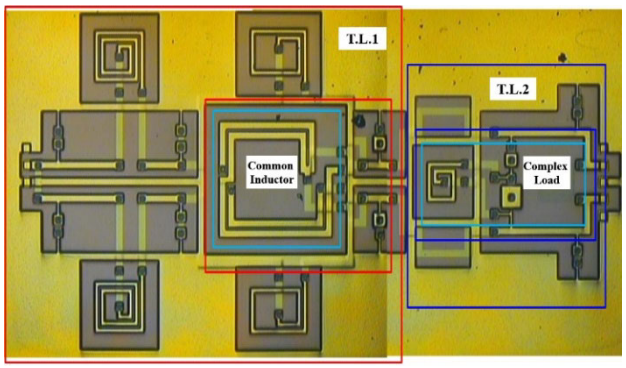

FIGURE 9. Image of the dual-band Wilkinson power divider with chip area, 4.5mm×2.2mm.

TABLE 1. Simulated transmission line properties of the layout.

Frequency (GHz)	T.L.1		T.L.2	
	Z_{01} (Ω)	θ_1 (°)	Z_{02} (Ω)	θ_2 (°)
1.8	46.3	64	22	36
2.4	53.2	88	23	49

TABLE 2. Simulated results of the common inductor and complex load.

Frequency (GHz)	Common inductor		Complex load	
	$L_{com,e}$ (nH)	$L_{com,o}$ (nH)	R_p (Ω)	C_p (pF)
1.8	2.1	0.53	10.5	4.1
2.4	2.1	0.53	28.4	2.4

Layout simulations used Momentum ADS from Keysight Technologies, Inc. The simulated results of each circuit components were listed in Table 1 and 2. Note that the characteristic impedance of T.L.1 varied from 46.3 Ω at 1.8 GHz to 53.2 Ω at 2.4 GHz while those of T.L.2 were quite constant. The simulated phase for T.L.1 at 2.4 GHz was 88°, close to that of the ideal transmission line of 86°. For T.L.2, the simulated phase at 2.4 GHz was 49°, compared to 48° for the ideal line. Simulated and measured results are shown in Fig. 10, which shows good agreement. Table 3 summarizes some simulated and measured S-parameters at both operating frequencies. At 1.8 GHz, the measured circuit performance differed a little from the simulation. However, at 2.4 GHz, the difference was greater, as the trends of measured S-parameter graphs deviated from those of the simulation. Overall, at both operating frequencies, the reflection at all ports were better than −11.9 dB, the isolations at the

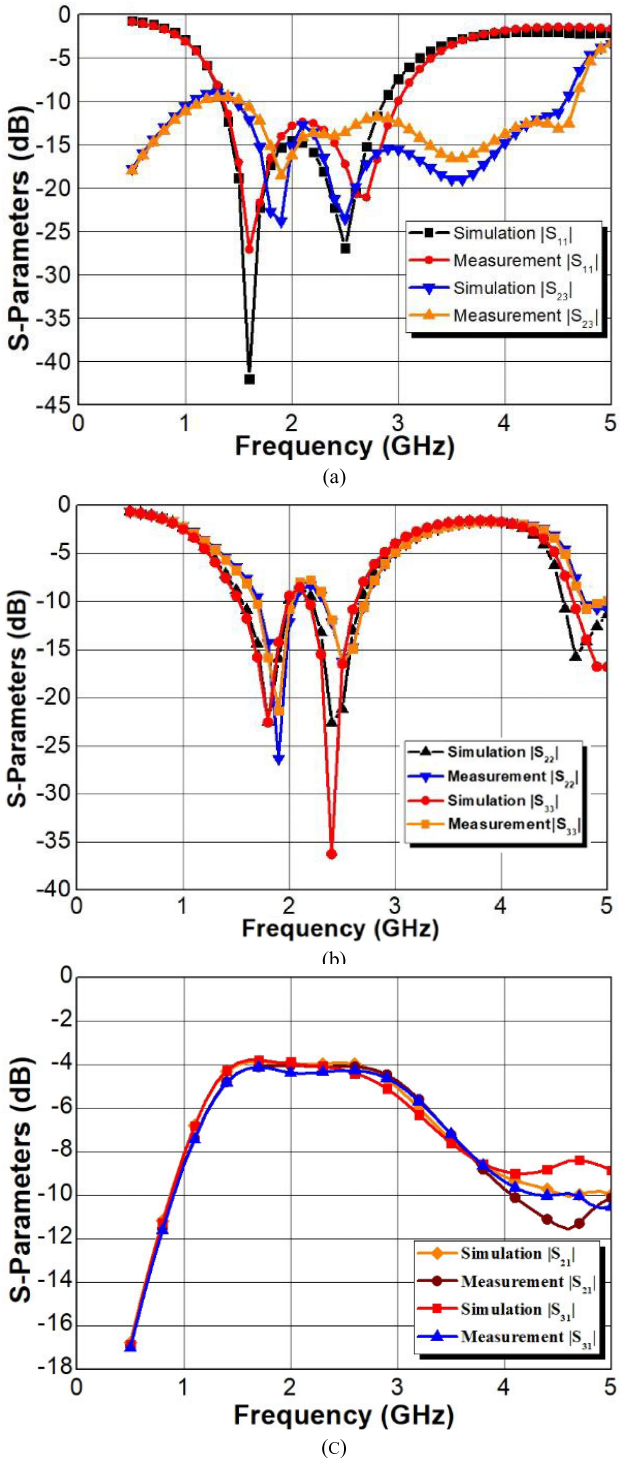

FIGURE 10. Comparison of layout simulation and measurement results of the designed circuit. (a) Input reflection and isolation, (b) output reflection and (c) transmission.

output ports were better than −14 dB and the transmission coefficients were better than −4.3 dB.

Table 4 summarizes previously reported power dividers. The $|S_{21}|$ or $|S_{31}|$ values from [12], [7], [8] and [9] were high because they were off-chip dual-band power dividers, where high Q components could be realized. However, the circuit sizes were large. Some other works were single-band power

TABLE 3. Summary of S-parameters from simulation and measurements.

Simulation/Measurement (dB)	Frequency (GHz)	
	1.8	2.4
$\|S_{11}\|$	−16.6/−16.5	−20.4/−15
$\|S_{22}\|$	−22/−14.3	−22/−12.1
$\|S_{33}\|$	−22/−16	−21.4/−11.9
$\|S_{23}\|$	−21/−15.2	−19.1/−14
$\|S_{21}\|$	−3.8/−4	−3.9/−4.1
$\|S_{31}\|$	-3.8/−4.1	−4.1/−4.3

TABLE 4. Comparison of previously reported works in literatures.

Reference	f_o (GHz)	$\|S_{21}\|$,$\|S_{31}\|$ (dB)	Return Loss (dB)	Isolation (dB)	Size (λ_0^2) ***
[20]	2.4	>-3.4	>15.2	38	3.128×10^{-5}**
[19]	0.9	>-3.7	>24	>19.6	10^{-4}
[22]	10	>-5.14	>16.61	26.88	9.9×10^{-5}
[12]	1/3.5	>-3.37	>18.4	>24.7	0.176*
[7]	1.1/2.55	>-3.5	>18	>17	4.94×10^{-2}**
[8]	1/2.5	>-3.31	>17.58	>17.05	0.172**
[9]	1/2.1	>-3.77	>20	>28*	8.68×10^{-2}*
This work	1.8/2.4	>-4.3	>11.9	>14	6.48×10^{-4}

*Estimated from the photograph, **Calculated from the dimensions provided, ***At the high frequency band

dividers so their sizes were smaller and performances better [19], [20], [22]. For dual-band dividers, in addition to dual-band circuit design criteria, there was a compromise between each frequency optimization, since component value variation and parasitics were added into a practical circuit. Therefore, the dual-band designs were generally larger. It is noted that this work generated smaller size than previous dual-band designs– see Table 4.

V. CONCLUSION

A compact 1.8/2.4-GHz dual-band Wilkinson power divider was designed and implemented in an integrated passive device process. To meet the circuit conditions at both frequencies, a common inductor and complex load were used with lumped transmission lines. The circuit parameters were determined by even and odd mode analysis of the circuit. For the even mode, the common inductor was used with lumped transmission lines to reduce the size of the circuit, while the input impedances of both ports were matched. In the odd mode, the complex load was used in addition to the lumped transmission lines and common inductor to match both ports. Overall, the simulated and measured results agreed well. For both frequencies, measured reflections at all ports were better than −11.9 dB, isolations at the output ports were better than −14 dB and transmission coefficients were better than −4.3 dB.

ACKNOWLEDGMENT

The authors would like to thank the National Chip Implementation Center (CIC), Hsinchu, Taiwan, for the chip fabrication and measurement support.

REFERENCES

[1] K. Rawat and F. M. Ghannouchi, "A design methodology for miniaturized power dividers using periodically loaded slow wave structure with dual-band applications," *IEEE Trans. Microw. Theory Techn.*, vol. 57, no. 12, pp. 3380–3388, Dec. 2009.
[2] Y. Wu, Y. Liu, and Q. Xue, "An analytical approach for a novel coupled-line dual-band Wilkinson power divider," *IEEE Trans. Microw. Theory Techn.*, vol. 59, no. 2, pp. 286–294, Feb. 2011.
[3] L. Wu, Z. Sun, H. Yilmaz, and M. Berroth, "A dual-frequency Wilkinson power divider," *IEEE Trans. Microw. Theory Techn.*, vol. 54, no. 1, pp. 278–284, Jan. 2006.
[4] M. J. Park and B. Lee, "Wilkinson power divider with extended ports for dual-band operation," *Electron. Lett.*, vol. 44, no. 15, pp. 916–917, Jul. 2008.
[5] M.-J. Park and B. Lee, "A dual-band Wilkinson power divider," *IEEE Microw. Wireless Compon. Lett.*, vol. 18, no. 2, pp. 85–87, Feb. 2008.
[6] K.-K.-M. Cheng and F.-L. Wong, "A new Wilkinson power divider design for dual band application," *IEEE Microw. Wireless Compon. Lett.*, vol. 17, no. 9, pp. 664–666, Sep. 2007.
[7] M. Kumar, S. K. Parui, and S. Das, "Design of miniaturized dual-band Wilkinson power divider using dual and cascade pi-shaped transmission lines," *Radioengineering*, vol. 27, no. 4, pp. 1056–1063, Dec. 2018.
[8] L. Xi and Y. Lin, "A novel design of dual-band Wilkinson power divider with simple structure and wide band-ratios characteristics," *J. Electromagn. Waves Appl.*, vol. 28, no. 13, pp. 1635–1641, Jul. 2014.
[9] X. Xu and X. Tang, "A design approach for dual-band Wilkinson power divider with two pairs of coupled-line sections," *PIER Lett.*, vol. 45, pp. 81–87, 2014.
[10] Y. Wu, Y. Liu, and X. Liu, "Dual-frequency power divider with isolation stubs," *Electron. Lett.*, vol. 44, no. 24, pp. 1407–1408, Nov. 2008.
[11] Z. B. Khan, Z. Huiling, and Z. Yimin, "A new simplified approach for design of dual-band Wilkinson power divider with two and three transmission line sections using only even-mode analysis," *J. Microw., Optoelectron. Electromagn. Appl.*, vol. 15, no. 4, pp. 390–401, Dec. 2016.
[12] F.-X. Liu and J.-C. Lee, "Design of new dual-band Wilkinson power dividers with simple structure and wide isolation," *IEEE Trans. Microw. Theory Techn.*, vol. 67, no. 9, pp. 3628–3635, Sep. 2019.
[13] A. Genc and R. Baktur, "Dual- and triple-band Wilkinson power dividers based on composite right- and left-handed transmission lines," *IEEE Trans. Compon., Packag., Manuf. Technol.*, vol. 1, no. 3, pp. 327–334, Mar. 2011.
[14] M. Zhao, A. Kumar, C. Wang, B. Xie, T. Qiang, and K. K. Adhikari, "Design method of dual-band Wilkinson power divider with improved out-of-band rejection performance and high design flexibility," *AEU-Int. J. Electron. C.*, vol. 110, pp. 1–7, Oct. 2019.
[15] M.-J. Chiang, H.-S. Wu, and C.-K. C. Tzuang, "A Ka-band COMS Wilkinson power divider using synthetic quasi-TEM transmission lines," *IEEE Microw Wireless Compon Lett.*, vol. 17, no. 12, pp. 837–839, Dec. 2007.
[16] E. Kaymaksut, Y. Gürbüz, and I. Tekin, "Impedance matching Wilkinson power dividers in 0.35 μm SiGe BiCMOS technology," *Microw. Opt. Technol. Lett.*, vol. 51, no. 3, pp. 681–685, Mar. 2009.
[17] L.-H. Lu, Y.-T. Liao, and C.-R. Wu, "A miniaturized Wilkinson power divider with CMOS active inductors," *IEEE Microw. Wireless Compon. Lett.*, vol. 15, no. 11, pp. 775–777, Nov. 2005.
[18] S. Wang and R.-X. Wang, "A tunable CMOS Wilkinson power divider using active inductors," *AEU-Int. J. Electron. Commun.*, vol. 66, no. 8, pp. 655–658, Aug. 2012.
[19] T. Qiang, C. Wang, and N.-Y. Kim, "A compact high-reliability high-performance 900-MHz WPD using GaAs-IPD technology," *IEEE Microw. Wireless Compon. Lett.*, vol. 26, no. 7, pp. 498–500, Jul. 2016.
[20] Y. Li, C. Wang, and N.-Y. Kim, "A high performance compact Wilkinson power divider using GaAs-based optimized integrated passive device fabrication process for LTE application," *Solid-State Electron.*, vol. 103, pp. 147–153, Jan. 2015.
[21] C. Pakasiri and T. Kongchayasukwat, "Improvement of transmission line circuit on lossy substrate with application on phase shifter design," in *Proc. 7th Int. Electr. Eng. Congr. (iEECON)*, Cham, Switzerland, Mar. 2019, pp. 1–4, Paper EL 43-46.
[22] K. Nithiporndecha, S. Wang, and C. Pakasiri, "Compact Wilkinson power divider using composite right/left-handed transmission line on CMOS process," in *Proc. 8th Int. Electr. Eng. Congr. (iEECON)*, Chiang Mai, Thailand, Mar. 2020, pp. 1–4.

CHATRPOL PAKASIRI was born in Bangkok, Thailand, in 1975. He received the B.S. degree in electronics engineering from the King Mongkut's Institute of Technology Ladkrabang, Bangkok, in 1996, and the M.S. and Ph.D. degrees from the Electrical and Computer Engineering Department, University of Houston, Texas, USA, in 2001 and 2005, respectively, and the M.S. degree from the EECS International Graduate School, National Chiao Tung University, Hsinchu, Taiwan, in 2013. Since 2014, he has been working as a Lecturer with the College of Advanced Manufacturing Innovation, King Mongkut's Institute of Technology Ladkrabang. His research interests include electromagnetics applications, antenna designs, microwave circuits, and RFIC design.

SEN WANG (Member, IEEE) received the B.S. degree in electrical engineering from National Taiwan University, Taipei, Taiwan, in 2004, and the M.S. and Ph.D. degrees from the Graduate Institute of Communication Engineering, National Taiwan University, in 2006 and 2009, respectively. He joined the Faculty of the Department of Electronic Engineering, National Taipei University of Technology, Taipei, as an Assistant Professor, in February 2010. He is currently a Professor. His research interests include the design of microwave and millimeter-wave passive circuits, CMOS RF integrated circuits, and radar system engineering.